

# Metamorphic devolatilization of subducted oceanic metabasalts: implications for seismicity, arc magmatism and volatile recycling

D.M. Kerrick<sup>a,\*</sup>, J.A.D. Connolly<sup>b</sup>

<sup>a</sup> *Department of Geosciences, The Pennsylvania State University, University Park, PA 16802, USA*

<sup>b</sup> *Earth Sciences Department, Swiss Federal Institute of Technology, 8092 Zurich, Switzerland*

Received 13 December 2000; received in revised form 13 April 2001; accepted 13 April 2001

---

## Abstract

Subducted oceanic metabasalts are believed to be a primary source of volatiles for arc magmatism and fluid-induced seismicity. From phase equilibria computed for an average oceanic metabasalt we present a model for subduction zone devolatilization for pressures up to 6 GPa ( $\sim 180$  km). Along high temperature geotherms complete dehydration occurs under forearcs, whereas dehydration does not occur along low temperature geotherms. For intermediate geotherms, major dehydration occurs under subarcs and provides a subjacent H<sub>2</sub>O source for arc volcanism. Decarbonation is negligible along cold and intermediate geotherms and limited along high temperature geotherms. Because decarbonation is limited for all subducted carbonate-bearing lithologies, transfer of CO<sub>2</sub> from subducted slabs to arc magmas may be triggered by aqueous fluid infiltration. Metabasalt devolatilization could induce seismicity in forearcs (high temperature geotherms) and subarcs (intermediate geotherms); however, because of the lack of devolatilization, metabasalts would not be a fluid source for seismicity with low temperature geotherms. Along low temperature geotherms, limited devolatilization of subducted oceanic metabasalts and marine sediments in forearcs and subarcs provides a mechanism for return of volatiles to the deeper mantle. © 2001 Elsevier Science B.V. All rights reserved.

*Keywords:* metabasalt; subduction; metamorphism; volatilization; carbon dioxide

---

## 1. Introduction

Devolatilization in subduction zones is essential to arc magmatism and volatile recycling. The principal volatile components (H<sub>2</sub>O and CO<sub>2</sub>) are contained in hydroxylated and carbonated

minerals within three protoliths: marine sediments, ophicarbonates, and metabasalts. Volatile components in the latter two lithologies are introduced by hydrothermal alteration at mid-ocean ridges (MORs) [1]. Computed high pressure phase equilibria relevant to subduction zone devolatilization of ophicarbonates and marine sediments are discussed in our other contributions [2,3]. This paper treats the remaining carbonate-bearing lithology (metabasalt) that is considered to be a primary source of volatiles for arc magmatism

---

\* Corresponding author. Tel.: +1-814-865-7574;  
Fax: +1-814-863-7823; E-mail: kerrick@geosc.psu.edu

[1,4–6]. Because of the importance of subduction zones to CO<sub>2</sub> recycling and the global carbon cycle, our studies on subduction zone devolatilization have targeted the release of CO<sub>2</sub> by metamorphic decarbonation. Nonetheless, our strategy also allows us to track the expulsion of H<sub>2</sub>O by metamorphic dehydration.

## 2. Protolith

In the oceanic crust most of the volatile components occur in metabasalts in the upper ~ 500 m [7,8]. We computed high pressure phase equilibria using Staudigel et al.'s [7] 'Super Composite' bulk rock composition (for the upper 550 m of oceanic crust). The CO<sub>2</sub> content of this bulk composition (2.95 wt%) is in close agreement with Alt and Teagle's [8] estimate for the upper ~ 500 m of hydrothermally altered oceanic crust.

## 3. Computational methodology

Our approach is analogous to that of our investigations on ophicarbonates [2] and marine sediments [3]. The stable phase relations for Staudigel et al.'s [7] 'Super Composite' metabasalt bulk composition (Table 1) were computed as a

function of pressure and temperature using free energy minimization [9]. The thermodynamic database of Holland and Powell [10] was used for the properties of all end member species, and mineral solutions were modeled as summarized in the Appendix. In addition to the phases that appear as stable phases in the phase diagram section shown in Fig. 1, alkali feldspar, biotite, chloritoid, carpholite, olivine and orthopyroxene solutions were considered in the calculations, but were not found to be stable at the *P–T* conditions considered herein. Thermodynamic data for H<sub>2</sub>O, CO<sub>2</sub>, and their mixtures were computed from the CORK equation of state [11].

The free energy minimization strategy employed for the calculations is described in [9] with modifications detailed by Connolly and Petriani [12]. The strategy differs from conventional computational techniques in that the continuous compositional variation of solutions is discretized at the onset of calculations. The discretization of solution compositions results in finite accuracy, the calculations reported here were carried out with a maximum allowed error of 1 mol% for binary mixing sites and 3 mol% for high order sites. The discretization of solution compositions leads, in turn, to discretization of high variance phase fields in computed phase diagram sections. Consequently, the phase relations of a section are represented by a continuous polygonal mesh of smaller fields within which the composition, abundances and physical properties of the stable phases are uniquely determined. The resulting phase diagram sections are useful for understanding the phase relations of complex metamorphic systems and for applications in which it is necessary to establish the variations in rock properties such as density, enthalpy, elastic moduli, and (as in this study) volatile contents through a metamorphic cycle. In comparison to current numerically exact techniques, our approach offers greater numerical stability and a more rational means of representing computed phase relations than can be obtained by conventional Gibbs energy minimization algorithms [13–16]. In contrast to the methods outlined by Holland and Powell [10] and Spear [17] our approach has the advantage that it is fully automated and that knowledge of

Table 1  
Chemical composition (wt%) of average MOR metabasalt ('Super Composite' from [7])

SiO <sub>2</sub>	45.8
TiO <sub>2</sub>	1.12
Al <sub>2</sub> O <sub>3</sub>	15.53
Fe <sub>2</sub> O <sub>3</sub>	10.02
MnO	0.17
MgO	6.66
CaO	12.88
Na <sub>2</sub> O	2.07
K <sub>2</sub> O	0.56
P <sub>2</sub> O <sub>5</sub>	0.11
H <sub>2</sub> O	2.68
CO <sub>2</sub>	2.95
Total	100.61

The bulk composition used for computing the phase diagram sections assumed all iron is ferrous and excluded MnO and P<sub>2</sub>O<sub>5</sub>.

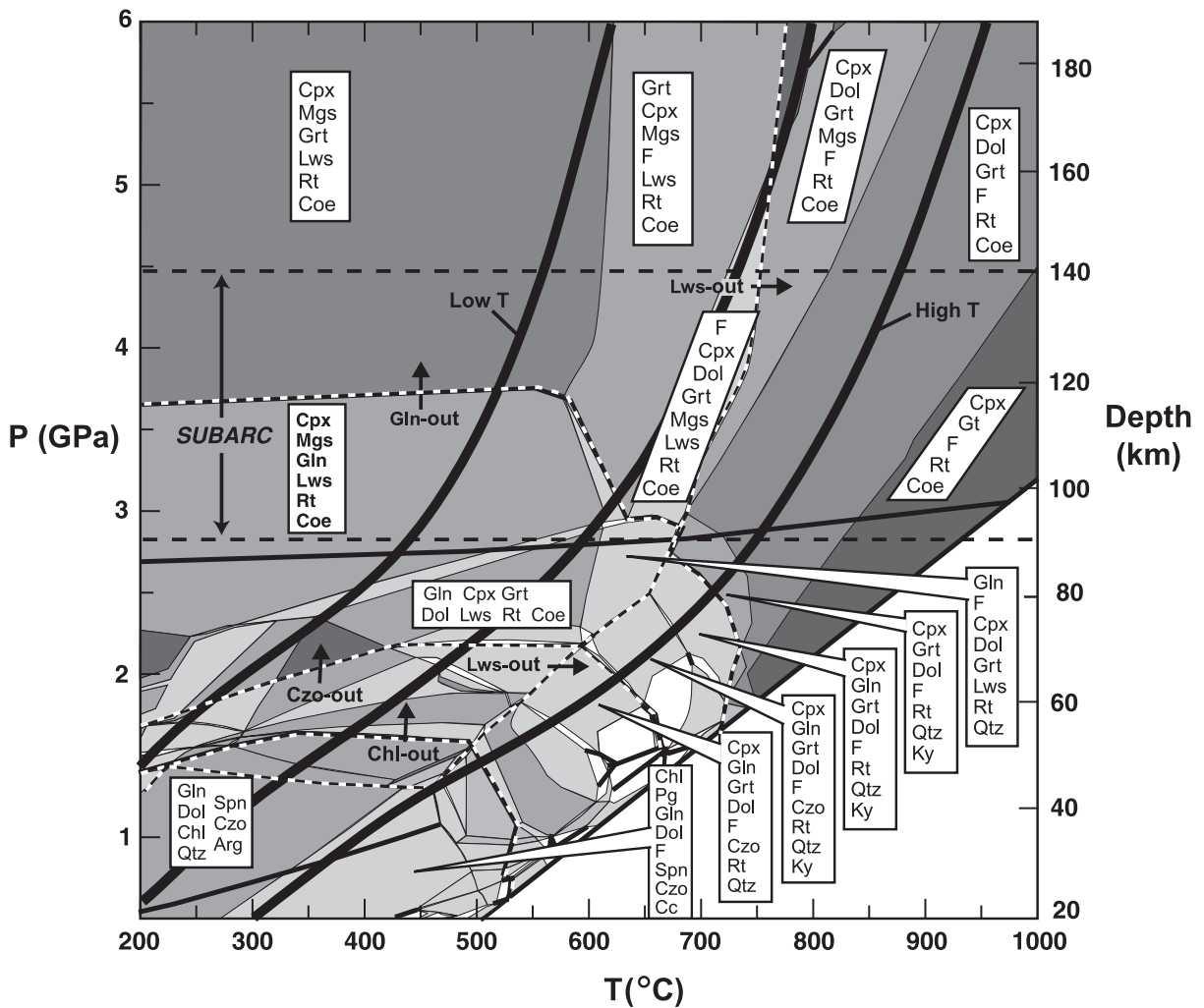


Fig. 1. Phase diagram section computed for Staudigel et al.'s [7] 'Super Composite' carbonate-bearing oceanic metabasalt bulk composition. Phase abbreviations [17]: Arg = aragonite, Cal = calcite, Chl = chlorite, Coe = coesite, Cpx = clinopyroxene, Czo = clinzoisite, Dol = dolomite, F = fluid, Gln = glaucophane, Grt = garnet, Ky = kyanite, Lws = lawsonite, Mgs = magnesite, Pg = paragonite, Qtz = quartz, Rt = rutile, Spn = sphene. Muscovite/phengite is present in all fields. The thick 'High T' and 'Low T' curves correspond to the respective geotherms for the upper surfaces of subducted slabs in SE and NW Japan [18]; the intermediate geotherm is midway between the high temperature and low temperature geotherms. The shading denotes the variance of the phase fields. Phase field boundaries corresponding to univariant equilibria are noted with heavy lines. The dashed lines and small arrows depict mineral disappearance ('out') in crossing phase field boundaries. Assemblages in the small fields at  $P < 1.5$  GPa and  $T < 500^\circ\text{C}$  are omitted for clarity. Subarc depth range is from [34].

the stable phase relations of a system is not a prerequisite for the construction of a phase diagram section. The approach is implemented as a component of a collection of Fortran computer programs for the calculation and graphical representation of petrological phase equilibria. This

package, including documentation and the thermodynamic data employed here, can be accessed via the Internet ([erdw.ethz.ch/~jamie/perplex.html](http://erdw.ethz.ch/~jamie/perplex.html)). The website also includes a tutorial outlining and explaining the steps necessary for the computation of Figs. 1–3.

## 4. Computational results

### 4.1. $P$ - $T$ phase equilibria

As shown in Fig. 1, there is a marked contrast between the  $P$ - $T$  slopes of the phase field boundaries below and above  $P \approx 3$  GPa. In particular, the  $P$ - $T$  region near the high temperature geotherm at  $P < 3$  GPa is characterized by phase field boundaries with negative slopes. Although the majority of phase field boundaries in the phase diagram section do not correspond to univariant equilibria, the ‘back bending’ is similar to the negative Clapeyron slopes of univariant devolatilization equilibria at elevated pressures. At lower temperatures the phase field boundaries have relatively shallow positive slopes. In contrast, the phase field boundaries at  $P > 3$  GPa have comparatively steep positive slopes.

### 4.2. Devolatilization

To track metamorphic devolatilization along the tops of subducted slabs we adopted Peacock and Wang’s [18] geotherms for the NW and SE Japan subduction zones (Fig. 1). These geotherms are reasonable approximations for the extremal geotherms likely to be realized in subduction zones (S.M. Peacock, personal communication).

The computed quantities of  $H_2O$  and  $CO_2$  retained in the metabasalt are shown in Figs. 2 and 3.

Along the high temperature geotherm, complete dehydration occurs under forearcs (depths  $< 85$  km) whereas relatively limited decarbonation is predicted (Fig. 3). The marked dehydration along the high temperature geotherm is attributed to its trajectory across phase fields bounded by negative  $P$ - $T$  slopes (Fig. 1). No devolatilization occurs along the lowest temperature geotherm (Fig. 3). For intermediate geotherms the depth range of

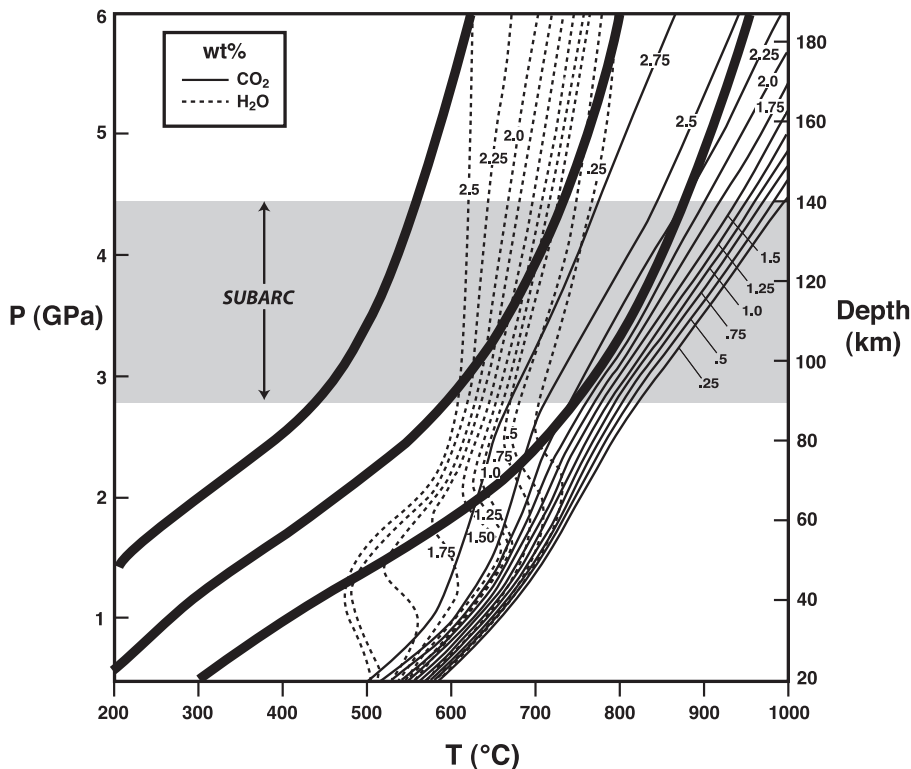


Fig. 2. Weight percentages of  $CO_2$  and  $H_2O$  in metabasalt. Thick curved lines are geotherms (see Fig. 1).

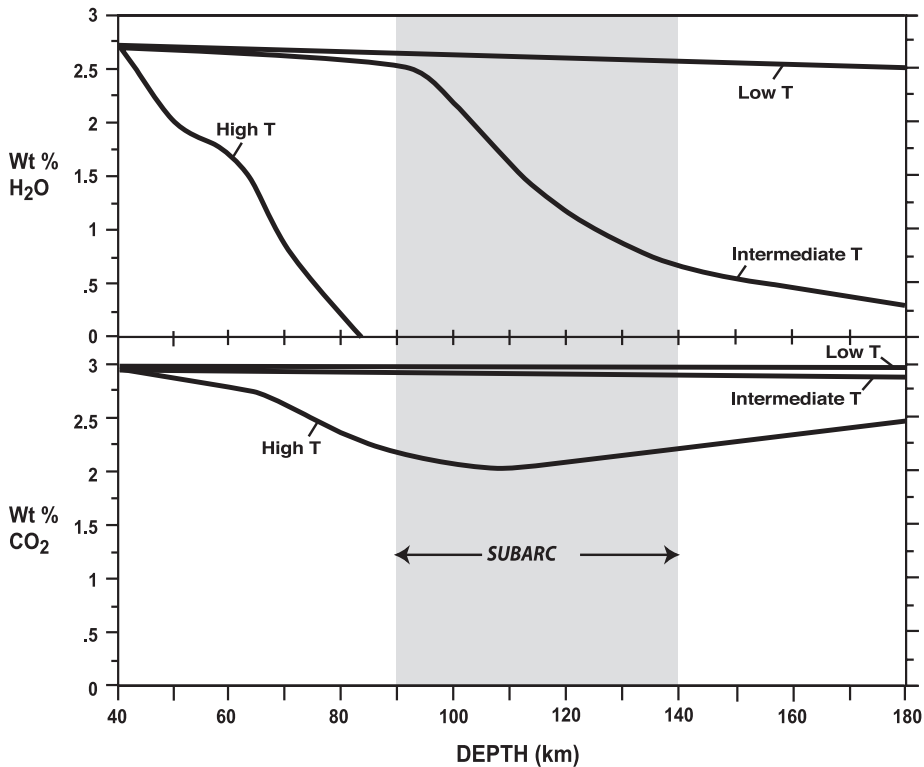


Fig. 3. Weight percentages of  $\text{CO}_2$  and  $\text{H}_2\text{O}$  in metabasalt along the three geotherms depicted in Figs. 1 and 2.

significant dehydration critically depends upon the geotherm. For a geotherm midway between the extremal geotherms, substantial dehydration occurs at subarc depths (Fig. 3).

## 5. Discussion

Our phase diagram section is not applicable to the entire range of compositions (and, thus, the range of mineral assemblages) in metabasalts. In particular, the high pressure phase equilibria for carbonate-free metabasalt protoliths, and the nature and compositions of fluids generated during metamorphism, will differ from that of the model composition considered in this study. Nevertheless, it is informative to make some generalized comparisons between the computed phase equilibria and those derived from experimental studies or inferred from natural metabasalt parageneses.

For subduction zone  $P$ – $T$  conditions, several

experimental studies have been carried out on carbonate-free MOR basalt [4–6]; however, experimental data on carbonate-bearing MOR basalt are very limited [19]. The computed upper stability of lawsonite is in agreement with experimental studies [6,20]. Our upper pressure limit for clinozoisite is  $\sim 0.8$  GPa less than that of Schmidt and Poli [6]. This discrepancy may be attributed to the presence of Fe in the experimentally produced zoisite and, thus, expansion of the zoisite stability field due to crystalline solution. The computed upper pressure limit for sodic amphibole (Fig. 1) is  $\sim 1$  GPa larger than that of experiments on  $\text{CO}_2$ -free metabasalts [4–6]. Expansion of the amphibole stability field in metabasalts by the addition of  $\text{CO}_2$  is compatible with experimental data [19]. As with clinozoisite/zoisite stability, differences in amphibole stability may be attributed to differences in amphibole composition. Our chlorite stability field is  $\sim 0.8$  GPa below that of Schmidt and Poli [6]. Compared to carbonate-

free systems, a reduction of the chlorite stability field is expected due to both reduced  $H_2O$  activity in the fluid phase and the sequestration of  $MgO$  in dolomite and magnesite. Chloritoid is a product in experimental studies of carbonate-free metabasalts [6,20] and it is common in eclogites [21,22]. However, chloritoid does not appear as a stable phase in our computed phase diagram section. The absence of a chloritoid stability field in this section is consistent with the absence of chloritoid in Molina and Poli's [19] experiments on  $CO_2$ -bearing metabasalts.

Regardless of the reasons for the discrepancies in the computed versus experimentally determined phase equilibria, uncertainties shrouding the  $P$ – $T$  stability of hydroxylated minerals will not substantially affect the general conclusions drawn from our computed phase equilibria. Thus, for example, with a comparatively smaller  $P$ – $T$  field of amphibole, as suggested by Schmidt and Poli [6], dehydration would be complete under forearc (as we conclude), albeit at a shallower depth than implied from our phase diagram section.

Our computed phase equilibria (Fig. 1) are generally consistent with petrologic data on metabasalts that have undergone high pressure (HP) and ultra-high pressure (UHP) metamorphism (blueschist and eclogite facies). Progressing toward higher pressures and temperatures the sequence of hydroxylated mineral disappearance (Fig. 1: chlorite  $\rightarrow$  clinozoisite  $\rightarrow$  glaucophane) is characteristic of natural high pressure parageneses [23]. Mineral assemblages in the higher pressure part of our phase diagram section are generally consistent with those of carbonate-bearing eclogites formed during UHP metamorphism [24,25]. Our computed stability of glaucophane is commensurate with the occurrence of glaucophane in coesite-bearing rocks [24]. Discrepancies between our phase diagram section and natural parageneses may be attributed to our closed system assumption and solution behavior that is not accounted for in our models. Because fluid saturation was not specified in our closed system computations, a fluid phase is absent throughout much of the lower temperature part of our phase diagram section. The lack of lawsonite and fluid in the lowest  $P$ – $T$  region of Fig. 1 is a consequence of the fact

that the water content of the system is too low to stabilize these phases. The abundance of lawsonite in glaucophane-bearing blueschists attests to higher  $H_2O$  activities than implied by our phase diagram section. However, fluid is present in the area of the phase diagram section (Fig. 1) coincident with the  $CO_2$  isopleths in Fig. 2. Consequently, Fig. 2 provides a model for fluid-present decarbonation. The rarity of lawsonite in eclogites does not necessarily contradict the broad stability of this phase in high pressure metabasalts as implied in this study and in experimental investigations [6,19]. Textures implying the transformation of lawsonite to epidote/clinozoisite in eclogites, coupled with clockwise  $P$ – $T$  paths of HP and UHP rocks [20], suggest that lawsonite is unlikely to be preserved in many eclogites. As discussed in the preceding paragraph, Fe in clinozoisite will expand the stability field of this phase and, thus, would allow clinozoisite to be stable with coesite as implied in UHP terranes [24].

The limited decarbonation of subducted metabasalts reflects the stability of magnesian carbonates at high pressure. In concert with experimental studies on carbonate-bearing metabasalts [19,26], the computed phase relations (Fig. 1) show a transition from calcite/aragonite  $\rightarrow$  dolomite  $\rightarrow$  magnesite with increasing pressure.

In addition to uncertainties in phase equilibria attributable to inaccuracies in thermochemical data and equations of state, our conclusions hinge upon the validity of Peacock and Wang's [18] limiting low temperature and (especially) high temperature geotherms. If future modeling reveals that the  $P$ – $T$  conditions of the limiting high temperature geotherm for subduction zones are similar to those adopted in this study, our conclusions will not be substantially altered. However, our conclusions will require modification if additional modeling demonstrates that the limiting high temperature geotherm is at higher temperatures than that adopted herein.

Our computation assumes closed system behavior. There are two limiting scenarios regarding open system behavior: (1) volatile loss only (no fluid infiltration) and (2) open to both loss and influx of volatiles. In comparison to closed system behavior, the case of volatile loss only (1) would

inhibit decarbonation because less solid phase reaction is necessary to buffer the fluid composition. Accordingly, with model (1) CO<sub>2</sub> expulsion from subducted metabasalts would be even less than that with closed system behavior. However, with the system open to the influx of volatiles (2), infiltration of H<sub>2</sub>O-rich fluids could drive decarbonation and thus enhance CO<sub>2</sub> loss. The implications of this are summarized in Section 6.

## 6. Conclusions

Our computed phase equilibria for carbonated metabasalts are consistent with Molina and Poli's [19] experimental study, i.e., decarbonation is restricted to higher temperature geotherms. We predict (Fig. 3) relatively limited CO<sub>2</sub> loss along the highest temperature geotherm. Phase equilibria suggest that ophicarbonates undergo little or no decarbonation during subduction [2]. We predict [3] that marls with initially high H<sub>2</sub>O/CO<sub>2</sub> ratios are the *only* protolith that undergoes substantial decarbonation in subduction zones (and only for intermediate to high temperature geotherms). Because H<sub>2</sub>O-rich marls are relatively restricted in most subduction zone trenches [27], these observations pose a 'carbonate dilemma', i.e., how is CO<sub>2</sub> for arc magmatism supplied to the mantle wedge? One possibility is melt transfer. However, experimental data suggest that clay-rich sediments [28] and carbonated metabasalts [26] do not undergo melting in subduction zones. Dissolution of subducted carbonates into aqueous fluids is a possible alternative mechanism for expulsion of significant quantities of CO<sub>2</sub>. Experiments at 1 GPa show considerable dissolution of calcite starting with pure H<sub>2</sub>O in the fluid phase [29]. However, because fluids in metacarbonate rocks are H<sub>2</sub>O–CO<sub>2</sub> fluid mixtures, the extent of decarbonation via carbonate dissolution in subducted carbonate-bearing metabasalts and metasediments is enigmatic.

A likely mechanism for supplying large quantities of CO<sub>2</sub> for arc volcanism is infiltration-induced decarbonation. Infiltration of H<sub>2</sub>O-rich fluids into carbonate lithologies is a well-established mechanism for inducing decarbonation reactions

[17]. Accordingly, H<sub>2</sub>O derived from dehydration of subducted serpentinites could result in decarbonation of overlying carbonate-bearing metabasalts and metasediments. There is controversy regarding the abundance and existence of serpentinites in the oceanic lithosphere of subduction zones [2]. If serpentinites do not exist in a subducted slab, H<sub>2</sub>O derived from dehydration of metabasalts could nevertheless induce decarbonation in the overlying carbonate-bearing metasediments.

Computations suggest that the amounts of subducted CO<sub>2</sub> and H<sub>2</sub>O are significantly less than the amounts of CO<sub>2</sub> and H<sub>2</sub>O emitted from arc volcanoes [30,31]. Consequently, a significant proportion of these volatiles are released in forearcs and/or subducted beyond subarcs. In the Marianas subduction zone, carbonate chimneys on the seafloor above serpentinite diapirs containing metabasalt xenoliths attest to decarbonation in forearcs of some subduction zones [32,33]. However, we do not necessarily contend that wholesale decarbonation of subducted metabasalts occurs in forearcs and subarcs. Carbonates in UHP eclogites [24] attest to incomplete decarbonation and, thus, retention of CO<sub>2</sub> in deeply subducted metabasalts, and imply that there has not been wholesale infiltration-induced decarbonation of subducted metabasalts.

Assuming that many subduction zones have geotherms intermediate between the limiting geotherms adopted here, subarc dehydration should be common in subducted metabasalts and serpentinites. Accordingly, the slab beneath most subarcs could be a source of H<sub>2</sub>O and CO<sub>2</sub> for arc magmas. As such, volatile transfer to the mantle wedge in forearcs, and subsequent downward drag of the carbonated and hydrated mantle wedge by corner flow [34,35], would not be required as a mechanism to supply volatiles for arc magmatism.

Dehydration of subducted metabasalts has been considered a source for fluid-induced seismicity [18,36]. In SW Japan (high temperature geotherm in Figs. 1–3) the maximum depth of intraslab earthquakes is 50–65 km whereas for NE Japan (low temperature geotherm in Figs. 1–3) the intraslab earthquakes reach a maximum frequency at

125 km and continue 200 km [18]. Peacock and Wang [18] concluded that the depth distribution of earthquake hypocenters in NW and SE Japan is consistent with phase equilibria for metabasalts. Indeed, the maximum depth of hypocenters in SW Japan is consistent with our phase equilibria along the high temperature geotherm that imply complete dehydration of metabasalt by  $\sim 85$  km (Fig. 3). However, we predict that to depths of  $\sim 180$  km, subducted metabasalts along the low temperature geotherm (for NW Japan) undergo no dehydration. Accordingly, earthquakes in the NW Japan subduction zone would not be attributed to fluid released from metamorphic devolatilization of subducted oceanic metabasalts. This does not, however, rule out metamorphic dehydration from other lithologies as a source of fluids for earthquakes in the NW Japan subduction zone. If the upper mantle in the subducted slab contains serpentinite, phase equilibria [2] imply that dehydration of this lithology could account for the abundant earthquakes at 100–150 km. We emphasize that a primary caveat of the foregoing conclusions is the validity of Peacock and Wang's [18] geotherms for tops of the subducted slabs in NW and SE Japan.

Because hydrothermal alteration is confined mostly to the upper 500 m of the oceanic crust [7,8], we confine our correlation of subduction zone seismicity and dehydration embrittlement to the uppermost part of subducted slabs. Dehydration-induced seismicity within the upper kilometer or so of subducted slabs is compatible with the concentration of earthquake hypocenters along the tops of the slabs [36]. However, we do not necessarily consider that dehydration embrittlement explains the hypocenter distribution in double seismic zones. It has been proposed [37] that the deeper slab hypocenters in double subduction zones (i.e., those 40–50 km below the tops of the subducted slabs) are caused by fluids released by dehydration of serpentinitized mantle ultramafics [37]. Peacock [37] contends that serpentinitization of the mantle to depths of 40–50 km below the slab surface occurs by the influx of water along faults at the lithospheric flexure below subduction zone trenches. Seismic pumping along shear zones is invoked as a mechanism for

penetration of fluid to such depths [37]. We question whether seismic pumping by deep earthquakes could create hydraulic gradients adequate to draw surface fluids to depths of 40–50 km.

As with Schmidt and Poli [6] our study implies that dehydration of subducted metabasalts is continuous. This reflects high variance of the devolatilization process as is also the case for subducted sediments [3]. Accordingly, dehydration is spread out over a depth zone and we do not expect pulses of fluid release (corresponding to univariant devolatilization) from subducted metabasalts and marine sediments. Because phase equilibria for metabasalts show that the blueschist  $\rightarrow$  eclogite transformation is largely multivariant, attempts to treat this transformation as a univariant process [18] should be viewed with caution. Continuous dehydration is consistent with the generally homogeneous distribution of earthquake hypocenters along the tops of subducted slabs [36].

Our equilibrium analysis implicitly assumes that there is no significant kinetic overstepping and metastability of metamorphic transformations. Although significant metastability and overstepping has been suggested for the transformation of anhydrous oceanic basalts and gabbros to eclogites [38], the catalytic effect of  $H_2O$  is likely to make equilibrium models appropriate for dehydrating systems such as metabasalts. From seismic wave velocities Abers [39] suggested metastable persistence of blueschists in metamorphosed oceanic crust subducted along low temperature geotherms. However, his interpretation neglected subducted metasediments above the oceanic metabasic rocks. Because of limited devolatilization along cold geotherms [3], deeply subducted metasediments could contribute to the low seismic velocities. Accordingly, we caution against using seismic velocity data to argue for metastability of metamorphic transformations in the subducted oceanic crust.

The depth of metamorphic devolatilization of all volatile-containing subducted lithologies is critically dependent upon the slab surface geotherm. There will be significant differences in the depth of decarbonation between subduction zones with high temperature versus low temperature upper slab geotherms. Furthermore, differences

in metamorphic devolatilization in various subduction zones are expected because of the significant variations in the amounts, lithologies and volatile contents of subducted sediments entering different subduction zones [27,40]. Differences in the extent and mineralogy of MOR hydrothermal alteration are predicted in slow versus fast spreading centers ([41,42], J. Alt, personal communication); thus, corresponding differences are expected in devolatilization of subducted metabasalts.

Geochemical modeling of the global carbon cycle assumes that arc CO<sub>2</sub> paleofluxes were correlative with the rates of subduction which were in turn correlated with the spreading rates at MORs [43,44]. The accuracy of such modeling is questionable in light of the predicted differences in metamorphic devolatilization for different subduction zones.

## Acknowledgements

This research was supported by National Science Foundation Grant 9975231 (MARGINS program). This paper was completed during J.A.D. Connolly's appointment at the Center for Advanced Studies, Norwegian Academy of Science and Letters, Oslo, Norway. We thank Simon Peacock for his advice regarding subduction zone geotherms, Jeffrey Alt for his insight on hydrothermal alteration of oceanic crust hydrothermal, and Jeffrey Alt, Juliette Forneris, John Holloway, and David Rubie for their thoughtful reviews. [RV]

## Appendix

The crystalline solution notation, solution compositions ( $w$ ,  $x$ ,  $y$ , and  $z$  are fractions that vary between zero and unity) and references for the solution models employed are:

Ab/Kf	Alkali (Na/K) feldspar, low structural state, Na <sub>x</sub> K <sub>y</sub> Ca <sub>1-x-y</sub> Al <sub>2-x-y</sub> Si <sub>2+x+y</sub> O <sub>8</sub> [45,46]
Bt	Biotite, KMg <sub>(3-y)x</sub> Fe <sub>(3-y)(1-x)</sub> Al <sub>1+2y</sub> Si <sub>3-y</sub> O <sub>10</sub> (OH) <sub>2</sub> [10]
Chl	Chlorite, Mg <sub>(5-y)x</sub> Fe <sub>(5-y)(1-x)</sub> Al <sub>2+2y</sub> Si <sub>3-y</sub> O <sub>10</sub> (OH) <sub>8</sub> [47]

Cpx	Low clinopyroxene, Na <sub>1-y</sub> Ca <sub>y</sub> Mg <sub>x</sub> Fe <sub>(1-x)y</sub> Al <sub>y</sub> Si <sub>2</sub> O <sub>6</sub> , modified from [48]
Dol	Dolomite–ankerite, CaMg <sub>x</sub> Fe <sub>(1-x)</sub> (CO <sub>3</sub> ) <sub>2</sub> [10]
Gt	Garnet, Fe <sub>3x</sub> Ca <sub>3y</sub> Mg <sub>3(1-x-y)</sub> Al <sub>2</sub> Si <sub>3</sub> O <sub>12</sub> [10]
Mgs	Magnesite–siderite, Mg <sub>x</sub> Fe <sub>(1-x)</sub> CO <sub>3</sub> [10]
Opx	Orthopyroxene, Mg <sub>2x</sub> Fe <sub>2-2x</sub> Si <sub>2</sub> O <sub>6</sub> [10]
Ms	Phengitic mica, K <sub>x</sub> Na <sub>1-x</sub> Mg <sub>y</sub> Fe <sub>z</sub> Al <sub>3-2(y+z)</sub> Si <sub>3+y+z</sub> O <sub>10</sub> (OH) <sub>2</sub> , modified from Chatterjee and Froese [49] and Holland and Powell [10]
Pl	Plagioclase, Na <sub>x</sub> Ca <sub>1-x</sub> Al <sub>2-x</sub> Si <sub>2+x</sub> O <sub>8</sub> [46]
TrTsPg	Amphibole (tremolite–tschermakite–pargasite), Ca <sub>2</sub> Na <sub>w</sub> Mg <sub>x</sub> Fe <sub>(1-x)</sub> Al <sub>3w+4y</sub> Si <sub>8-2w-2y</sub> O <sub>22</sub> (OH) <sub>2</sub> , modified from Holland and Powell [10]
TrTsGl	Amphibole (tremolite–tschermakite–glaucophane), Ca <sub>2-2z</sub> Na <sub>sz</sub> Mg <sub>x</sub> Fe <sub>(1-x)</sub> Al <sub>3w+4y</sub> Si <sub>8-2w-2y</sub> O <sub>22</sub> (OH) <sub>2</sub> , modified from Holland and Powell [10]

## References

- [1] J.C. Alt, Subseafloor processes in mid-ocean ridge hydrothermal systems, in: S.E. Humphris, R.A. Zierenberg, L.S. Mullineaux, R.E. Thompson (Eds.), Seafloor Hydrothermal Systems, Physical, Chemical, Biological, and Geological Interactions, Am. Geophys. Union Geophys. Monogr. 91 (1995) 85–114.
- [2] D.M. Kerrick, J.A.D. Connolly, Subduction of ophiicarbonates and recycling of CO<sub>2</sub> and H<sub>2</sub>O, *Geology* 26 (1998) 375–378.
- [3] D.M. Kerrick, J.A.D. Connolly, Metamorphic devolatilization of subducted marine sediments implications for CO<sub>2</sub> and H<sub>2</sub>O recycling, *Nature* 411 (2001) 293–296.
- [4] A.R. Pawley, J.R. Holloway, Water sources for subduction zone volcanism: new experimental constraints, *Science* 260 (1993) 664–667.
- [5] J. Liu, S.R. Bohlen, W.G. Ernst, Stability of hydrous phases in subducting oceanic crust, *Earth Planet. Sci. Lett.* 143 (1996) 161–171.
- [6] M.W. Schmidt, S. Poli, Experimentally based water budgets for dehydrating slabs and consequences for arc magma generation, *Earth Planet. Sci. Lett.* 163 (1998) 361–379.
- [7] H. Staudigel, S. Hart, H. Schmincke, B. Smith, Cretaceous ocean crust at DSDP Sites 417 and 418: Carbon uptake from weathering versus loss by magmatic outgassing, *Geochim. Cosmochim. Acta* 53 (1989) 3091–3094.
- [8] J.C. Alt, D.A.H. Teagle, The uptake of carbon during alteration of ocean crust, *Geochim. Cosmochim. Acta* 63 (1999) 1527–1535.
- [9] J.A.D. Connolly, Multivariable phase diagrams: an algorithm based on generalized thermodynamics, *Am. J. Sci.* 290 (1990) 666–718.
- [10] T.J.B. Holland, R. Powell, An internally consistent thermodynamic data set for phases of petrological interest, *J. Met. Geol.* 16 (1998) 309–343.

- [11] T.J.B. Holland, R. Powell, A compensated Redlich-Kwong (CORK) equation for volumes and fugacities of CO<sub>2</sub> and H<sub>2</sub>O in the range 1 bar to 50 kbar and 100–1600°C, *Contrib. Mineral. Petrol.* 109 (1991) 265–273.
- [12] J.A.D. Connolly, K. Petrini, A strategy for calculation of phase diagram sections and retrieval of rock properties as a function of physical conditions, *J. Met. Geol.*, submitted.
- [13] S.K. Saxena, G. Eriksson, Theoretical computation of mineral assemblages in pyrolite and lherzolite, *J. Petrol.* 24 (1983) 538–555.
- [14] B.J. Wood, J.R. Holloway, A thermodynamic model for subsolidus equilibria in the system CaO-MgO-Al<sub>2</sub>O<sub>3</sub>-SiO<sub>2</sub>, *Geochim. Cosmochim. Acta* 66 (1984) 159–176.
- [15] C. DeCapitani, T.H. Brown, The computation of chemical equilibria in complex systems containing non-ideal solutions, *Geochim. Cosmochim. Acta* 51 (1987) 2639–2652.
- [16] G. Eriksson, K. Hack, Chemsage – a computer program for the calculation of complex chemical equilibria, *Metall. Trans. B21B* (1990) 1013–1023.
- [17] F.S. Spear, Metamorphic phase equilibria and pressure-temperature-time paths, *Mineral. Soc. Am. Monogr.*, 1993, 798 pp.
- [18] S.M. Peacock, K. Wang, Seismic consequences of warm versus cool subduction metamorphism: Examples from southwest and northeast Japan, *Science* 286 (1999) 937–939.
- [19] J.F. Molina, S. Poli, Carbonate stability and fluid composition in subducted oceanic crust: an experimental study on H<sub>2</sub>O-CO<sub>2</sub>-bearing basalts, *Earth Planet. Sci. Lett.* 176 (2000) 295–310.
- [20] S. Poli, M.W. Schmidt, The high-pressure stability of hydrous phases in orogenic belts: an experimental approach on eclogite-forming processes, *Tectonophysics* 273 (1997) 169–184.
- [21] K. Bucher, M. Frey, *Petrogenesis of Metamorphic Rocks*, Springer-Verlag, Berlin, 1994, 318 pp.
- [22] B. Messiga, M. Scambelluri, G.B. Piccardo, Chloritoid-bearing assemblages in mafic systems and eclogite-facies hydration of alpine Mg-Al metagabbros (Erro-Tobbio Unit, Ligurian Western Alps), *Eur. J. Mineral.* 7 (1995) 1149–1167.
- [23] W.G. Ernst, J.L. Mosenfelder, M.L. Leech, J. Liu, H<sub>2</sub>O recycling during continental collision: Phase-equilibrium and kinetic considerations, in: B.R. Hacker, J.G. Liou (Eds.), *When Continents Collide: Geodynamics and Geochemistry of Ultra-High-Pressure Rocks*, Chapman and Hall, New York, 1998, pp. 275–295.
- [24] J. Liou, R. Zhang, W. Ernst, Occurrences of hydrous and carbonate phases in ultrahigh-pressure rocks from east-central China: implications for the role of volatiles deep in subduction zones, *Island Arc* 4 (1995) 362–375.
- [25] R.G. Coleman, X. Wang, *Ultrahigh-Pressure Metamorphism*, Cambridge University Press, Cambridge, 1995, 528 pp.
- [26] G.M. Yaxley, D.H. Green, Experimental demonstration of refractory carbonate-bearing eclogite and siliceous melt in the subduction regime, *Earth Planet. Sci. Lett.* 128 (1994) 313–325.
- [27] T. Plank, C.H. Langmuir, The chemical composition of subducting sediment and its consequences for the crust and mantle, *Chem. Geol.* 145 (1998) 325–394.
- [28] M.C. Johnson, T. Plank, Dehydration and melting experiments constrain the fate of subducted sediments, *Geochim. Geophys. Geosyst.* 1 (2000) 1525–2027.
- [29] N. Caciagli, C. Manning, Calcite solubility in water at high temperature and pressure: implications for the geochemistry of dense aqueous fluids, *Trans. Am. Geophys. Union (EOS)* 46 (1999) F1157.
- [30] G.E. Bebout, The impact of subduction-zone metamorphism on mantle-ocean chemical cycling, *Chem. Geol.* 126 (1995) 191–218.
- [31] D.M. Kerrick, Present and past non-anthropogenic CO<sub>2</sub> degassing from the solid Earth, *Rev. Geophys.* (2001) in press.
- [32] P. Fryer, M. Mottl, L. Johnson, J. Haggerty, S. Phipps, H. Maekawa, Serpentine bodies in the forearc of western Pacific convergent margins: origin and associated fluids, *Am. Geophys. Union Geophys. Monogr.* 88 (1995) 259–279.
- [33] H. Maekawa, P. Fryer, A. Ozaki, Incipient blueschist-facies metamorphism in the active subduction zone beneath the Mariana forearc, *Am. Geophys. Union Geophys. Monogr.* 88 (1995) 281–289.
- [34] Y. Tatsumi, S. Eggins, *Subduction Zone Magmatism*, Blackwell, Oxford, 1995, 211 pp.
- [35] H. Iwamori, Transportation of H<sub>2</sub>O and melting in subduction zones, *Earth Planet. Sci. Lett.* 160 (1998) 65–80.
- [36] S. Kirby, E.R. Engdahl, R. Denlinger, Intermediate-depth intraslab earthquakes and arc volcanism as physical expressions of crustal and uppermost mantle metamorphism in subducting slabs, in: G.E. Bebout, D.W. Scholl, S.H. Kirby, J.P. Platt (Eds.), *Subduction Top to Bottom*, Am. Geophys. Union Geophys. Monogr. 96 (1996) 195–214.
- [37] S.M. Peacock, Are the lower planes of double seismic zones caused by serpentine dehydration in subducting oceanic mantle?, *Geology* 29 (2001) 299–302.
- [38] B.R. Hacker, Eclogite formation and the rheology, buoyancy, seismicity, and H<sub>2</sub>O content of oceanic crust, in: G.E. Bebout, D.W. Scholl, S.H. Kirby, J.P. Platt (Eds.), *Subduction Top to Bottom*, Am. Geophys. Union, Geophys. Monogr. 96 (1996) 337–346.
- [39] G.A. Abers, Hydrated subducted crust at 100–250 km depth, *Earth Planet. Sci. Lett.* 176 (2000) 323–330.
- [40] D.K. Rea, L.J. Ruff, Composition and mass flux of sediment entering the world's subduction zones: Implications for global sediment budgets, great earthquakes, and volcanism, *Earth Planet. Sci. Lett.* 140 (1996) 1–12.
- [41] K.M. Gillis, Controls on hydrothermal alteration in a section of fast-spreading oceanic crust, *Earth Planet. Sci. Lett.* 134 (1995) 473–489.
- [42] H. Bougalt, J.-L. Charlou, Y. Fouquet, H.D. Needham, N. Vaslet, P. Appriou, P.J. Babbiste, P.A. Rona, L. Dmi-

- triev, S. Silantiev, Fast and slow spreading ridges: structure and hydrothermal activity, ultramafic topographic highs, and CH<sub>4</sub> output, *J. Geophys. Res.* 98 (1993) 9643–9651.
- [43] R.A. Berner, GEOCARB II: A revised model of atmospheric CO<sub>2</sub> over Phanerozoic time, *Am. J. Sci.* 294 (1994) 56–91.
- [44] E. Tajika, Climate change during the last 150 million years: Reconstruction from a carbon cycle model, *Earth Planet. Sci. Lett.* 160 (1998) 695–707.
- [45] J.B. Thompson, D.R. Waldbaum, Mixing properties of sanidine crystalline solutions. IV. Phase diagrams from equations of state, *Am. Mineral.* 54 (1969) 811–838.
- [46] R.C. Newton, T.V. Charlu, O.J. Kleppa, Thermochemistry of the high structural state plagioclases, *Geochim. Cosmochim. Acta* 44 (1980) 933–941.
- [47] T. Holland, J. Baker, R. Powell, Mixing properties and activity-composition relationships of chlorites in the system MgO-FeO-Al<sub>2</sub>O<sub>3</sub>-SiO<sub>2</sub>-H<sub>2</sub>O, *Eur. J. Mineral.* 10 (1998) 395–406.
- [48] T. Gasparik, Experimental study of subsolidus phase relations and mixing properties of pyroxene and plagioclase in the system Na<sub>2</sub>O-CaO-Al<sub>2</sub>O<sub>3</sub>-SiO<sub>2</sub>, *Contrib. Mineral. Petrol.* 89 (1985) 346–357.
- [49] N.D. Chatterjee, E. Froese, A thermodynamic study of the pseudo-binary join muscovite-paragonite in the system KAlSi<sub>3</sub>O<sub>8</sub>-NaAlSi<sub>3</sub>O<sub>8</sub>-Al<sub>2</sub>O<sub>3</sub>-H<sub>2</sub>O, *Am. Mineral.* 60 (1975) 985–993.